JOURNAL OF THERMOPHYSICS AND HEAT TRANSFER
Vol. 13, No. 4, October–December 1999

Behavior of Two-Temperature Model in Intermediate Hypersonic Regime

Michiko Furudate,* Satoshi Nonaka,* and Keisuke Sawada†
Tohoku University, Sendai 980-8579, Japan

Shock standoff distance for a sphere is calculated to examine the behavior of the existing two-temperature model in the intermediate hypersonic flow regime. Calculations are carried out for three binary scaling parameter values, corresponding to nearly frozen, nonequilibrium, and nearly equilibrium flows, respectively. The obtained shock standoff distances are compared with the experimental data obtained in a ballistic range. It is shown that the two-temperature model reproduces the shock standoff distances in the intermediate hypersonic flows fairly well but tends to lose its accuracy where vibrational excitation occurs but chemical reactions are nearly frozen.

Nomenclature

M = collision partner in dissociation/recombination reactions
p_∞ = static pressure in the test section, Pa
q = power on the vibrational temperature in the definition of T_a, $0 < q < 1$
R = nose radius of a sphere, m
T = translational temperature, K
T_a = rate-controlling temperature for dissociation reactions, $T^{1-q}T_v^q$, K
T_v = vibrational temperature, K
U_∞ = flight velocity, m/s
γ = specific heat ratio
ρ_∞ = freestream density, kg/m^3

Introduction

VARIOUS air-breathing engine-powered launch systems are being studied in Japan. Such systems are planned to perform their flight in the intermediate hypersonic regime from 2.5 to 4.5 km/s in speed. To design such vehicles, computational fluid dynamics (CFD) codes that can accurately simulate real gas effects are needed. This is because chemical reactions in the shock layer can affect the pressure distribution and, thus, the aerodynamic characteristics of the vehicle. Moreover, because chemical reactions absorb a considerable amount of heat and reduce temperature in the boundary layer, the separation point, if it occurs, can be changed, possibly affecting the performance of the engine inlet. Experimental measurement of these real gas effects, however, is costly, and, therefore, CFD analysis is preferred if it could be made reliably.

CFD simulations have been successfully carried out mainly for high hypersonic nonequilibrium flows such as the flow occurring at the maximum heating point along the reentry trajectory. However, in a lower speed regime, it is uncertain whether the existing thermochemical models are able to reproduce the thermochemical states in the shock layer flow accurately. It is known that the existing two-temperature model,[1] which is commonly used in hypersonic CFD codes, can successfully reproduce thermochemical nonequilibrium phenomena in the high hypersonic regime. This is because only one vibrational temperature, that is, the temperature corresponding to nitrogen molecules, exists in the shock layer. In the lower speed range, postshock gas temperature is not very high, and so inadequate molecular dissociation occurs in the shock layer. Because different molecular species can have different vibrational temperatures, the validity of the two-temperature model in this flow regime becomes questionable.

One approach to validate the thermochemical model in CFD codes is to compare the shock standoff distance for a sphere with the experimental data measured in a ballistic range.[2] The shock standoff distance varies inversely with the density of gas in the shock layer, which in turn depends on the degree of chemical reaction and thermal excitation. Therefore, the shock standoff distance can serve as a reference value for validation of thermochemical model for air.

The ultimate purpose of the present study is to establish a multitemperature thermochemical model suitable for simulations of the lower hypersonic flow, that is, the speed range between 2.5 and 4.5 km/s, wherein all three molecules, N_2, O_2, and NO, can exist, which can be called the intermediate hypersonic regime. Toward this goal, we focus on the existing two-temperature model to examine its performance in the prediction of the thermochemical nonequilibrium state in the intermediate hypersonic regime. We employ the latest experimental data for shock standoff distances obtained at the ballistic range at the Shock Wave Research Center, Institute of Fluid Science, Tohoku University.[3–5]

Method of Calculation

The governing equations are the three-dimensional Navier–Stokes equations, consisting of global mass, species mass, momentum, total energy, and vibrational-electronic energy conservation equations.

Five neutral air species, N_2, O_2, N, O, and NO, are considered. By utilizing the concept of elementary conservation in which the ratio of oxygen and nitrogen atoms is kept constant everywhere, two-species conservation equations can be removed from the set of governing equations.[6] This assumption is valid even for viscous flow calculation if the net diffusion velocities for the oxygen and nitrogen atoms are identical, which is nearly true in air. Therefore, conservation equations for N, O, and NO are solved.

The following five chemical reactions are considered:

$$\begin{aligned} O_2 + M &\leftrightarrow O + O + M \\ N_2 + M &\leftrightarrow N + N + M \\ NO + M &\leftrightarrow N + O + M \\ N_2 + O &\leftrightarrow NO + N \\ NO + O &\leftrightarrow O_2 + N \end{aligned}$$

We employ the two-temperature model of Park to determine reaction rate coefficients.[7] According to this model, the rate coefficients for dissociation reactions due to two-body collisions are a function of the geometric-averaged temperature between translational and vibrational temperatures, that is, $\sqrt{TT_v}$. The vibrational energy equation accounts for the preferential removal or disposal of

Presented as Paper 99-0223 at the AIAA 37th Aerospace Sciences Meeting, Reno, NV, 11–14 January 1999; received 5 February 1999; revision received 30 June 1999; accepted for publication 11 July 1999.

*Graduate Student, Department of Aeronautics and Space Engineering, Aobayama 01. Student Member AIAA.

†Professor, Department of Aeronautics and Space Engineering, Aobayama 01. Senior Member AIAA.

highly excited vibrational states in dissociation or recombination. The degree of that is defined to be 30% of the dissociation energy. The translational–vibrational relaxation rates are given by the Landau–Teller equation.

The molecular viscosity for air species is given by the Blottner et al. model[8] and the thermal conductivity by Eucken's relation.[9] Those transport properties for air are obtained from Wilke's empirical formula.[10] We assume the diffusion coefficients to be constant for all species with constant Schmidt number of 0.5.

The present scheme is based on the cell-vertex finite volume method.[11] We employ a prismatic unstructured mesh system. The treatment is fully three dimensional. This enables us to avoid the possible mesh singularity often appearing near the stagnation point in the structured mesh system and also to provide higher spatial accuracy in the boundary-layer region. The convective numerical flux is calculated by one of the advection upwind splitting method (AUSM-DV) schemes.[12] The dependent variables along the mesh lines normal to the body surface are interpolated by the conventional MUSCL approach for structured meshes,[13] and Barth's method[14] is used in each unstructured mesh layer.

A two-level second-order accurate explicit Runge–Kutta method is used for time integration. The diagonal point implicit method[15] is employed for improving stability in the integration of the source terms. For convergence acceleration, the local time-stepping method is employed.

Experiment

The experiments are conducted using a two-stage light-gas gun ballistic range at the Shock Wave Research Center, Institute of Fluid Science, Tohoku University. In a ballistic range, because the projectile flies in a quiescent atmosphere, the freestream conditions can be characterized completely. The ballistic range, therefore, can provide reliable experimental data for validating hypersonic CFD codes.

The facility is shown schematically in Fig. 1. The ballistic range consists of a powder chamber, a 60-mm-bore pump tube 3 m in length, a high-pressure coupling, a 30-mm-bore launch tube 4 m in length, and a test chamber. The sequence of ballistic range operations is as follows: A high-density polyethylene piston accelerated by the explosion product gas of smokeless powder compresses helium gas in the pump tube. The compressed high-temperature helium ruptures the steel diaphragm and accelerates the model in the launch tube. The model flies in the test chamber and, finally, crashes into a steel bumper. In the test chamber, the flight velocity of the model is determined by measuring the time for the model to cross two laser beams located at an interval of 1 m.

The shadowgraph and schlieren methods are employed for flow visualization. The light source used in this study is a Nd-YAG laser of 5-ns pulse duration. The trigger timing of the laser pulse is adjusted using a delay circuit. The circuit measures the time interval for the model to pass between two pressure transducers separated by 1 m. The delay time is adjusted to trigger the laser pulse on the arrival of the projectile at test section.

To avoid possible contamination of the test gas in the test section by oil vapor, first the test section is evacuated by the turbomolecular pump below about a fraction of 1/10,000th of the test condition pressure. Then uncontaminated air is supplied into the test section. The pressure in the test section is measured by a mercury manometer.

Test Conditions

The experimental measurements of the shock standoff distances are conducted for several different binary scaling parameters.[16]

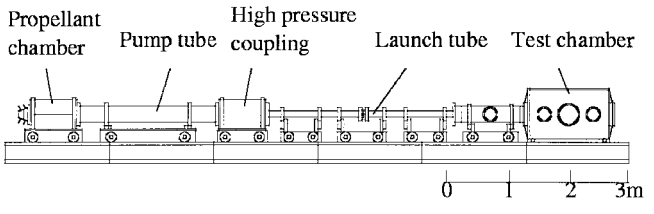

Fig. 1 Schematic of ballistic range.

Table 1 Test conditions

Case	$\rho_\infty R$, kg/m^2	R, mm	ρ_∞, kg/m^3	p_∞, Pa	U_∞, km/s
1-1	1.0×10^{-4}	14	0.00714	600	2.63
1-2	1.0×10^{-4}	15	0.00667	560	2.93
1-3	1.0×10^{-4}	7	0.0143	1,200	3.85
2-1	2.0×10^{-4}	14	0.0143	1,200	2.63
2-2	2.0×10^{-4}	15	0.0133	1,120	3.15
2-3	2.0×10^{-4}	7	0.0286	2,400	3.64
3-1	1.7×10^{-3}	14	0.121	10,130	2.56
3-2	1.7×10^{-3}	7	0.243	20,260	3.16

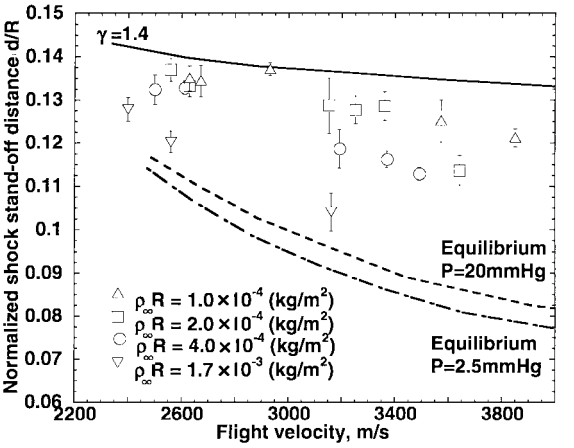

Fig. 2 Shock standoff distances for sphere measured in ballistic range.[3–5]

The binary scaling parameter is defined here as the product of the freestream density ρ_∞ and the radius of sphere R. The flows having the same binary scaling parameter can be considered as chemically similar flow where two-body dissociation reactions are dominant. Four different values of the binary scaling parameter are chosen to determine the experimental conditions corresponding to the nearly frozen, the nonequilibrium, and the nearly equilibrium flow regimes. Figure 2 summarizes the shock standoff distances for a sphere obtained in the experiment. The solid line shows the shock standoff distance for a perfect gas with $\gamma = 1.4$, whereas the two broken lines are for air in full chemical equilibrium.[17]

In the calculation, we consider three different binary scaling parameters chosen from the experimental conditions and, also, two or three different velocities for each parameter value. These conditions, 8 cases in total, are summarized in Table 1. The test gas is air consisting of 23.3% oxygen and 76.7% nitrogen by mass. Freestream temperature is 293 K. For all cases, we assume a noncatalytic isothermal wall of 1000 K. All meshes used in the calculations have 2678 points on the wall surface and 51 points in the normal direction. Mesh points along the radial mesh lines are clustered to the shock position to attain higher spatial resolution. A typical example of the present mesh system is shown in Fig. 3.

Results

Figure 4 shows the comparison of the calculated density contours and experimental schlieren photographs for the representative cases in each flow regime. Good agreements are obtained for the shock standoff distances in these results. One can see that the shock standoff distance tends to increase when the binary scaling parameter is decreased, approaching the frozen flow. This tendency is also observed in the experimental data.

Results for Nearly Frozen Flows

The calculated shock standoff distances for the three different velocities with a fixed binary scaling parameter of 1.0×10^{-4} are

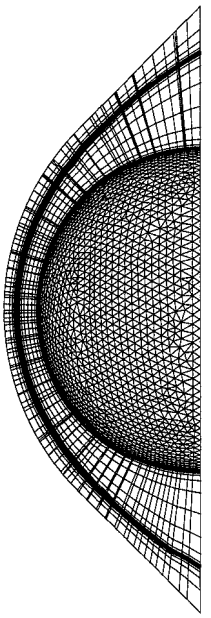

Fig. 3 Example of computational mesh system.

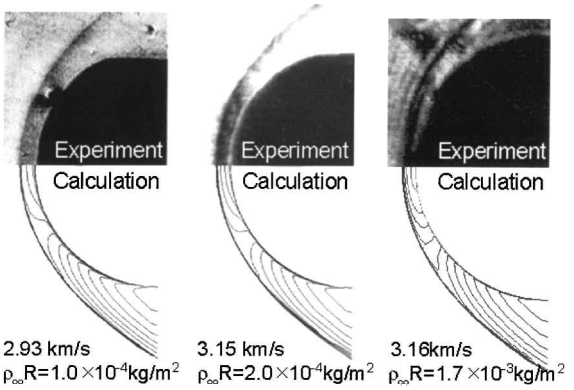

Fig. 4 Comparison of experimental schlieren photographs and calculated density contours.

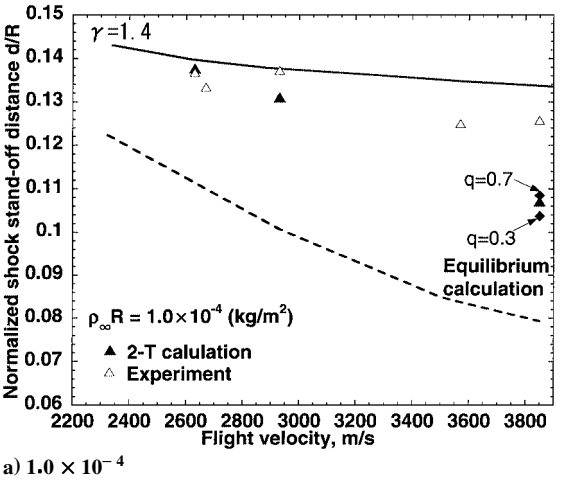

a) 1.0×10^{-4}

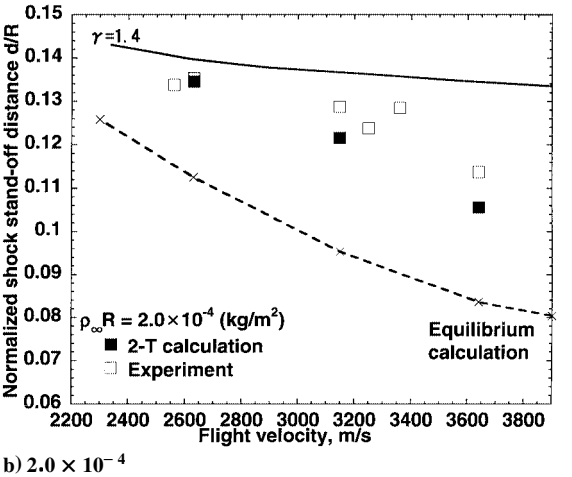

b) 2.0×10^{-4}

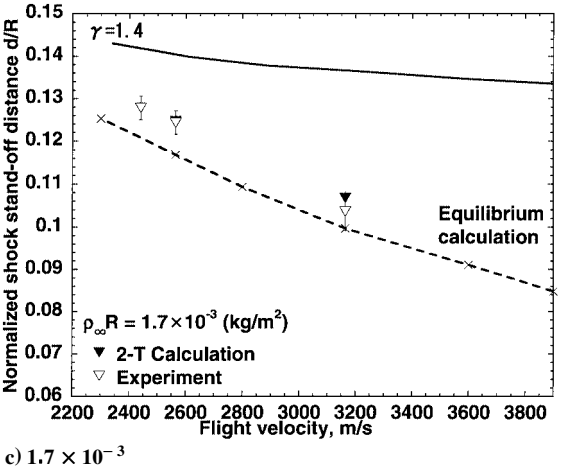

c) 1.7×10^{-3}

Fig. 5 Calculated and experimental shock standoff distances for sphere for three different $\rho_\infty R$ (kg/m^2).

shown in Fig. 5a. The solid line in Fig. 5a shows the frozen limit corresponding to the ideal gas solution with $\gamma = 1.4$, whereas the broken line shows the equilibrium limit obtained through the equilibrium flow calculations. Experimental results suggest that these flowfields are actually in a nearly frozen state.

For this binary scaling parameter value, a fair agreement with experiment is obtained for the lowest velocity (case 1-1). However, the calculated shock standoff distance gradually departs from the experimental value as the flight velocity increases (cases 1-2 and 1-3). Particularly in case 1-3, the departure becomes substantial. The corresponding distributions of the species mole fraction and the temperature along the stagnation streamline are shown in Figs. 6 and 7, respectively. One can see that the flowfields in cases 1-2 and 1-3 are chemically frozen, and thermal equilibrium is not reached even at the boundary-layer edge. The vibrational temperatures in these cases are rather low so that the dissociation reaction of O_2 molecules is not likely to occur. However, in case 1-3, the situation is quite different. A sizable amount of O_2 molecules actually dissociates in the shock layer, resulting in the presence of O, N, and NO. The vibrational temperature for this case reaches about 5000 K in the shock layer, and the thermal equilibrium is obviously reached at the boundary-layer edge.

To find the possible cause of the observed distinction between the calculated and the measured shock standoff distances for case 1-3, the following two numerical experiments are conducted. First, calculations are carried out in which the power q on the vibrational temperature in the definition of T_a is changed to see the coupling effect between vibrational temperature and chemical reactions. As seen in Fig. 5a, the shock standoff distance is decreased by 3% when $q = 0.3$. This is because the smaller value of q elevates T_a higher behind the shock wave. More dissociation reactions then occur in the shock layer, as shown in Fig. 6c, resulting in the lower translational temperature, as seen in Fig. 7c. If we assume $q = 0.7$, then T_a decreases behind the shock wave resulting in fewer chemical reactions because of the longer incubation period. This, however, increases the shock standoff distance by only less than 1%. These results indicate the calculated shock standoff distances are not very sensitive to the value of q. Second, calculations are carried out in which pure O_2 and pure N_2 flows are assumed. In Fig. 8a, the mole fraction

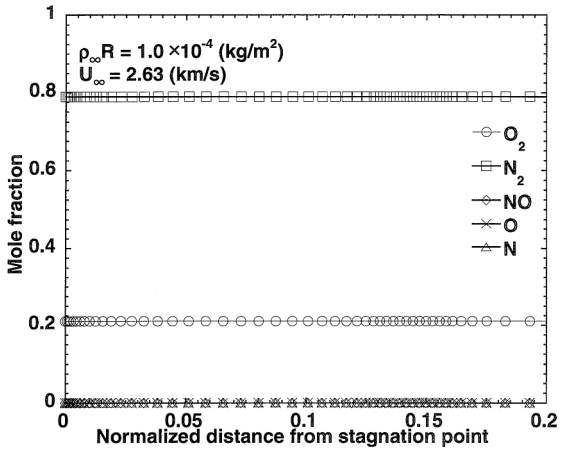

a) Case 1-1

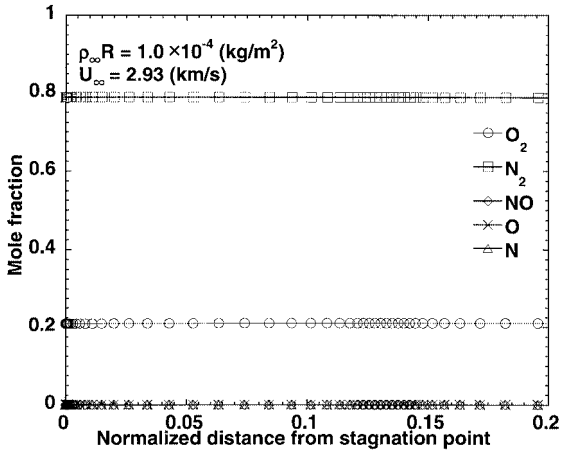

b) Case 1-2

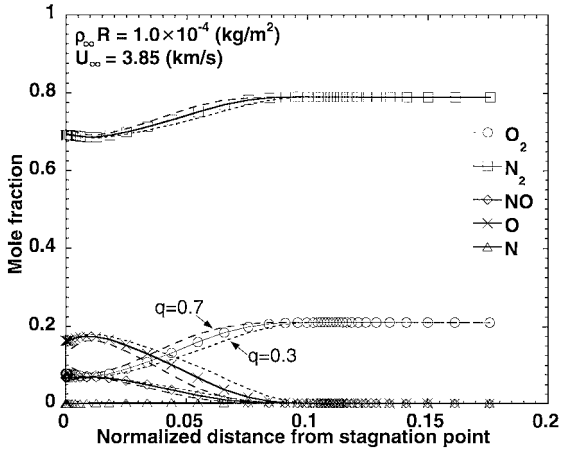

c) Case 1-3

Fig. 6 Species mole fraction profiles along the stagnation streamline.

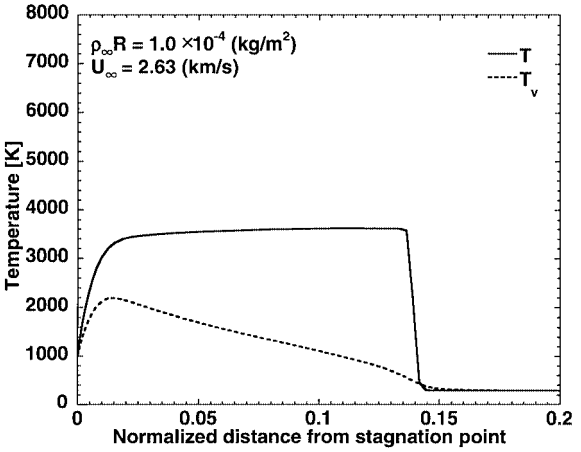

a) Case 1-1

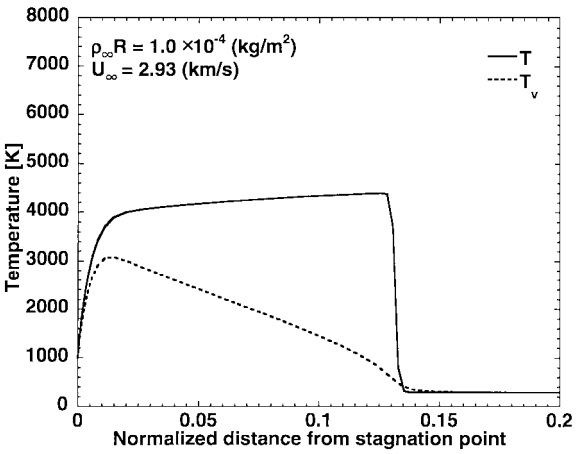

b) Case 1-2

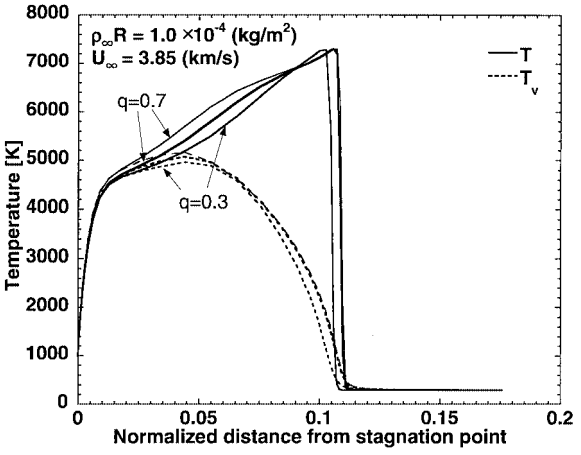

c) Case 1-3

Fig. 7 Temperature profiles along the stagnation streamline.

along the stagnation streamline for these test cases are shown. In a pure O_2 flow, a significant dissociation of O_2 molecules actually occurs. Conversely, a pure N_2 flow seems chemically frozen even for this flow condition. The corresponding temperature profiles are shown in Fig. 8b. For a pure O_2 flow, the thermal equilibration is accomplished rapidly behind the shock wave but not at all for a pure N_2 flow. These results indicate that the characteristics of the vibrational excitation of O_2 and N_2 molecules for this speed range are quite different. The shorter shock standoff distance obtained in the calculation for case 1-3 implies that the effect of the artificially excited vibrational mode of N_2 molecules due to the higher vibrational temperature given by the present two-temperature model exceeds the effect of lowered vibrational temperature of O_2 molecules. Note that the shock standoff distance for a pure N_2 flow almost agrees with the experimental data for air shown in Fig. 5a. This implies the N_2 molecules in the corresponding flowfield for air should be nearly chemically frozen as well as nearly vibrationally frozen.

Results for Nonequilibrium Flows

The obtained results for the binary scaling parameter of 2.0×10^{-4} are shown in Fig. 5b. For this binary scaling parameter, the calculated shock standoff distance agrees well with the corresponding experimental data for the lowest-velocity case (case 2-1). On the other hand, in the higher-speed range (cases 2-2 and 2-3), departures from the experimental data can be seen. This tendency is

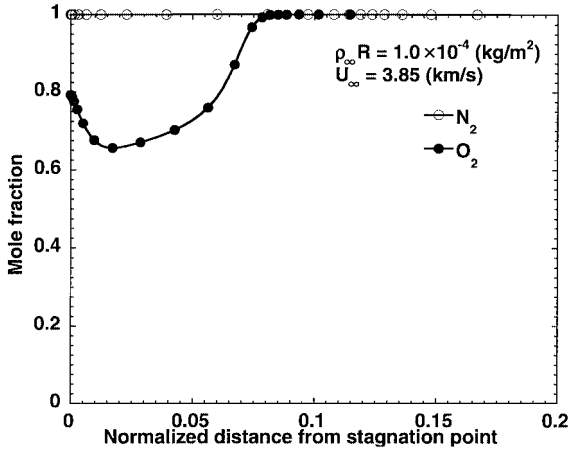

a) Species mole fraction

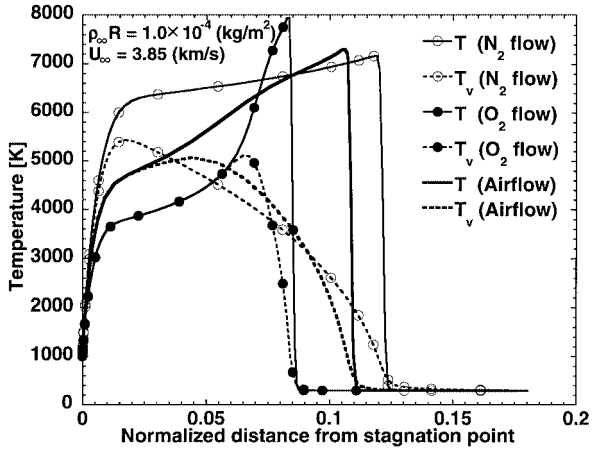

b) Temperature

Fig. 8 Profiles along the stagnation streamline for pure N_2 flow and O_2 flow.

quite similar to the preceding frozen cases. However, the departure, even for the highest-velocity case, is still moderate.

Corresponding mole fraction and temperature profiles are shown in Figs. 9 and 10. One can see the flowfield is obviously chemically frozen in case 2-1. Vibrational excitation slightly occurs but does not reach thermal equilibrium in the entire region. The present calculation, therefore, can reproduce the experimental value quite well, as in the frozen case. In case 2-2, the vibrational temperature is raised almost to 4000 K at the boundary-layer edge, where thermal equilibrium seems to be reached. The dissociation reaction of O_2 molecules begins to occur, resulting in the presence of O, N, and NO in the shock layer. In case 2-3, the overall temperature profiles are quite similar to those in case 1-3.

A mesh convergence study is carried out for case 2-2. In Fig. 10b, the temperature profiles calculated by using 31 mesh points and 71 mesh points in the normal direction are shown. Although the shock wave is slightly smeared for the case with 31 mesh points, the shock location and the temperature profiles agree well with those cases with 51 or 71 mesh points. The species mole fractions obtained by using different meshes are also compared, but no discernable difference is seen in the profiles. Therefore, they are not shown in Fig. 9b. These results indicate that the present 51 mesh points in the normal direction can provide virtually mesh-converged solutions.

Results for Nearly Equilibrium Flows

The shock standoff distances for the binary scaling parameter of 1.7×10^{-3} are compared in Fig. 5c. The experimental data are distributed near the equilibrium limit shown by the broken line. This confirms the flows are in nearly equilibrium state.

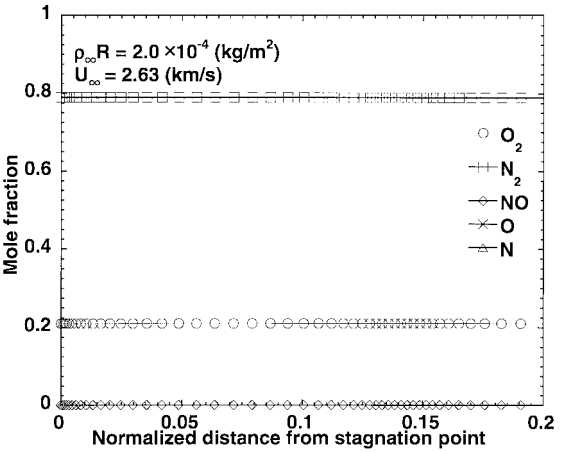

a) Case 2-1

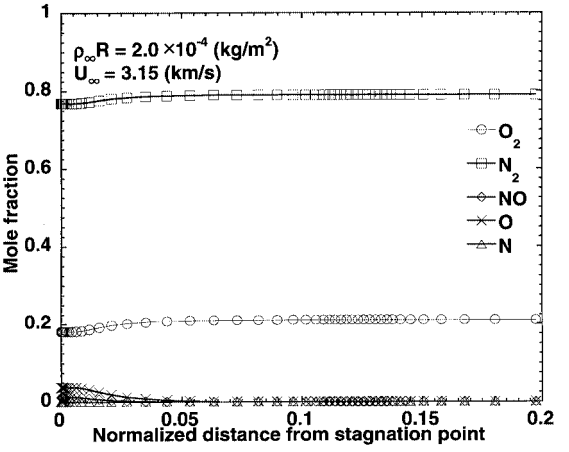

b) Case 2-2

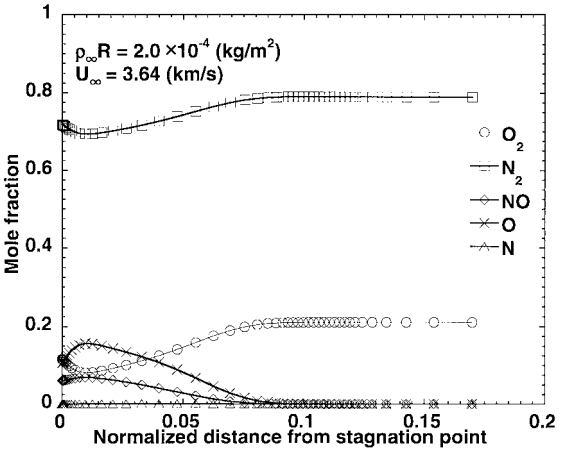

c) Case 2-3

Fig. 9 Species mole fraction profiles along the stagnation streamline.

Fair agreements between the calculated and experimental shock standoff distances are seen, even for higher flight speed. Corresponding mole fraction and temperature profiles are shown in Figs. 11 and 12. The flowfield in case 3-1 is chemically frozen. The thermal equilibration is, however, delayed almost to the boundary-layer edge, despite the larger binary scaling parameter. In case 3-2, the dissociation reaction of O_2 molecules occurs, and thermal equilibrium is reached immediately behind shock wave.

Discussion

For the lowest velocity cases from the three distinct flow regimes (cases 1-1, 2-1, and 3-1), the calculated shock standoff distances agree well with the experimental results. Calculated results indicate

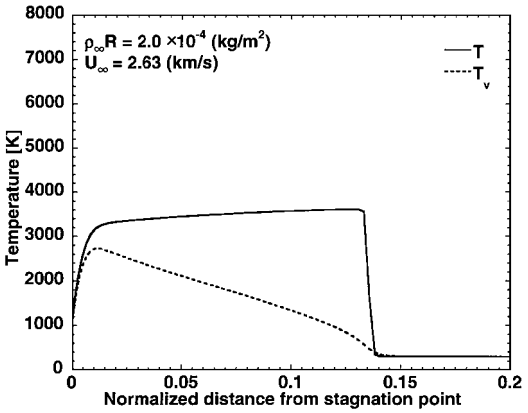

a) Case 2-1

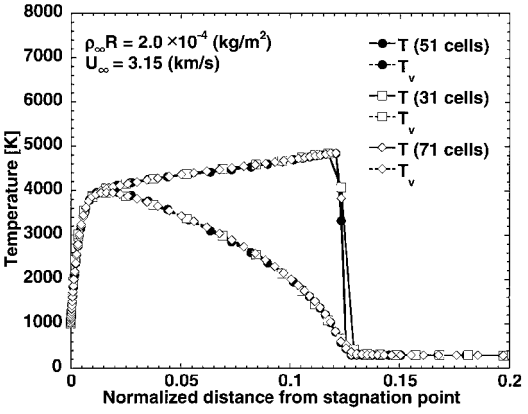

b) Case 2-2

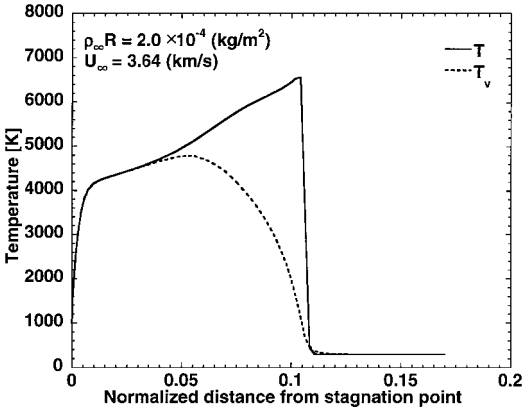

c) Case 2-3

Fig. 10 Temperature profiles along the stagnation streamline.

that these flowfields are all nearly chemically frozen. This is because the temperature rise behind the shock wave is too low to initiate dissociation. The vibrational temperature profiles are all similar to one another. The vibrational excitation gradually takes place behind the shock wave, but thermal equilibrium is never reached. The resulting flowfield can be well described by the two-temperature model because the amount of vibrational energy is still small.

For the highest-velocity cases covering nearly frozen to nonequilibrium flow regimes (cases 1-3 and 2-3), the agreement with the experiment is seen to be degraded. In particular, a substantial difference is seen in case 1-3. Numerical experiments have revealed that 1) the coupling effect between vibrational excitation and chemical reactions in the two-temperature model is not able to explain the observed distinction for this case and 2) a pure N_2 flow gives better agreement with the experimental data for air, suggesting that N_2 molecules in air should be nearly vibrationally frozen as well as chemically frozen for a dissociation reaction.

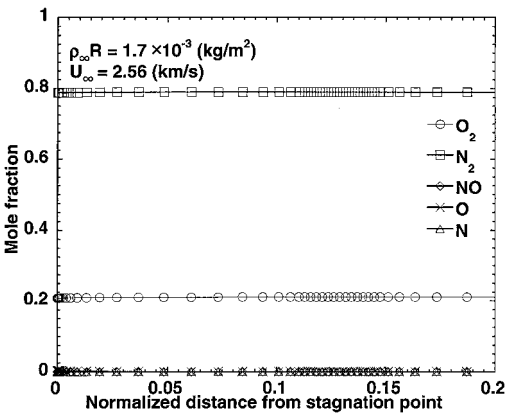

a) Case 3-1

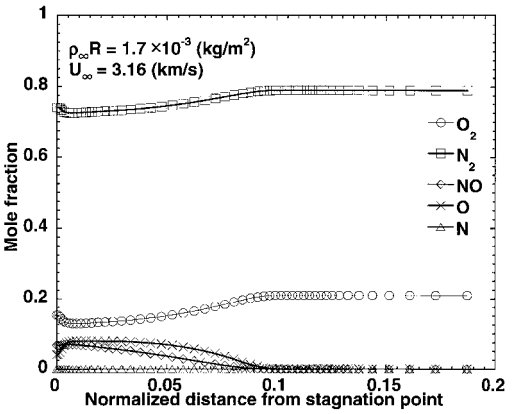

b) Case 3-2

Fig. 11 Species mole fraction profiles along the stagnation streamline.

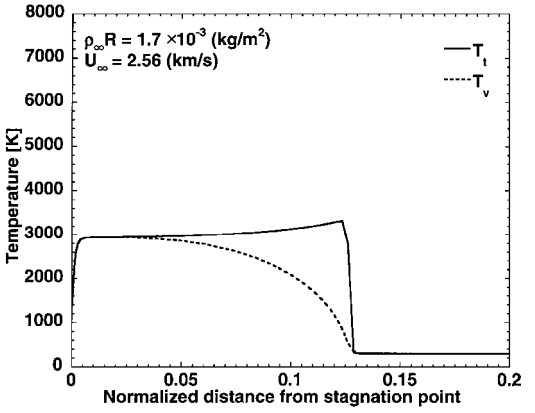

a) Case 3-1

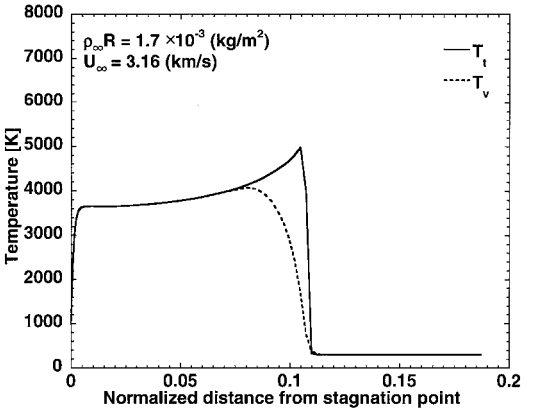

b) Case 3-2

Fig. 12 Temperature profiles along the stagnation streamline.

It is, therefore, interesting to observe from these results that the two-temperature model tends to lose its accuracy in intermediate hypersonic flows where considerable vibrational excitation occurs but chemical reactions are nearly frozen. As stated in the preceding section, this may be caused by assigning a common vibrational temperature to O_2, N_2, and NO molecules. If this is the case, a multi-temperature model assigning different vibrational temperatures to these molecules should be tried to improve agreement.

Conclusions

The shock standoff distances for a sphere are calculated to assess the validity of two-temperature model in the intermediate hypersonic speed regime. The following conclusions are obtained in this study:

1) The two-temperature model generally reproduces the shock standoff distances.

2) The two-temperature model, however, seems to lose its accuracy in the intermediate hypersonic flows when vibrational excitation occurs but chemical reaction are nearly frozen. This suggests that the assignment of a single vibrational temperature to different molecular species is no longer adequate to describe the flowfields in this regime.

Acknowledgments

The authors express their sincere thanks to Kazuyoshi Takayama, Shock Wave Research Center, Institute of Fluid Science, Tohoku University, for releasing the ballistic range data prior to their publication. They are also very much indebted to Chul Park for valuable suggestions.

References

[1]Park, C., "Assessment of Two-Temperature Kinetic Model for Ionizing Air," *Journal of Thermophysics and Heat Transfer*, Vol. 3, No. 3, 1989, pp. 233–244.

[2]Park, C., "Validation of CFD Codes for Real-Gas Regime," AIAA Paper 97-2530, June 1997.

[3]Nonaka, S., and Takayama, K., "Measurement of Shock Stand-Off Distance for Sphere in Ballistic Range," AIAA Paper 97-0563, Jan. 1997.

[4]Nonaka, S., and Takayama, K., "Overview of Ballistic Range Program at Tohoku University," AIAA Paper 98-2604, June 1998.

[5]Nonaka, S., Mizuno, H., and Takayama, K., "Ballistic Range Measurement of Shock Shapes in Intermediate Hypersonic Regime," AIAA Paper 99-1025, Jan. 1999.

[6]Park, C., *Nonequilibrium Hypersonic Aerothermodynamics*, Wiley, New York, 1989, pp. 145–170.

[7]Park, C., "A Review of Reaction Rates in High Temperature Air," AIAA Paper 89-1740, June 1989.

[8]Blottner, F. G., Johnson, M., and Ellis, M., "Chemically Reacting Viscous Flow Program for Multi-Component Gas Mixture," Sandia National Lab., Rept. SC-RR-70-754, Albuquerque, NM, Dec. 1971.

[9]Vincenti, W. G., and Kruger, C. H., *Introduction to Physical Gas Dynamics*, Wiley, New York, 1967, pp. 375–435.

[10]Wilke, C. R., "A Viscosity Equation for Gas Mixtures," *Journal of Chemical Physics*, Vol. 18, No. 4, 1950, pp. 517–519.

[11]Niizuma, K., and Sawada, K., "Nonequilibrium Flow Computations for the Space Shuttle Nose Using Unstructured Meshes," AIAA Paper 97-2548, June 1997.

[12]Wada, Y., and Liu, M. S., "A Flux Splitting Scheme with High-Resolution and Robustness for Discontinuities," AIAA Paper 94-0083, Jan. 1994.

[13]Anderson, W. K., Thomas, J. L., and Van Leer, B., "Comparison of Finite Volume Flux Vector Splittings for the Euler Equations," *AIAA Journal*, Vol. 24, No. 9, 1986, pp. 1453–1460.

[14]Barth, T. J., "Aspect of Unstructured Grid and Finite-Volume Solvers for the Euler and Navier–Stokes Equations," R-787, AGARD, May 1992, pp. 6/1–6/61.

[15]Eberhardt, S., and Imlay, S., "Diagonal Implicit Scheme for Computing Flows with Finite Pate Chemistry," *Journal of Thermophysics and Heat Transfer*, Vol. 6, No. 2, 1992, pp. 208–216.

[16]Anderson, J. D., Jr., *Hypersonic and High Temperature Gas Dynamics*, McGraw–Hill, New York, 1989, pp. 548–590.

[17]Lobb, R. K., "Experimental Measurement of Shock Detachment Distance on Sphere Fired in Air at Hypervelocities," *The High Temperature Aspects of Hypersonic Flow*, edited by W. C. Nelson, Pergamon, New York, 1964, pp. 519–527.